molecular pharmaceutics

Article

pubs.acs.org/molecularpharmaceutics

# Nanocrystal Dissolution Kinetics and Solubility Increase Prediction from Molecular Dynamics: The Case of α-, β-, and γ-Glycine

Conor Parks,[†] Andy Koswara,[†] Hsien-Hsin Tung,[‡,§] Nandkishor K. Nere,[‡] Shailendra Bordawekar,[‡] Zoltan K. Nagy,[†] and Doraiswami Ramkrishna*[,†]

[†]School of Chemical Engineering, Purdue University, 480 West Stadium Mall, West Lafayette, Indiana 47907, United States

[‡]Process Research & Development, AbbVie, Inc., 1 North Waukegan Road, North Chicago, Illinois 60064, United States

Supporting Information

**ABSTRACT:** Nanocrystals are receiving increased attention for pharmaceutical applications due to their enhanced solubility relative to their micron-sized counterpart and, in turn, potentially increased bioavailability. In this work, a computational method is proposed to predict the following: (1) polymorph specific dissolution kinetics and (2) the multiplicative increase in the polymorph specific nanocrystal solubility relative to the bulk solubility. The method uses a combination of molecular dynamics and a parametric particle size dependent mass transfer model. The method is demonstrated using a case study of α-, β-, and γ-glycine. It is shown that only the α-glycine form is predicted to have an increasing dissolution rate with decreasing particle size over the range of particle sizes simulated. On the contrary, γ-glycine shows a monotonically increasing dissolution rate with increasing particle size and dissolves at a rate 1.5 to 2 times larger than α- or β-glycine. The accelerated dissolution rate of γ-glycine relative to the other two polymorphs correlates directly with the interfacial energy ranking of $\gamma > \beta > \alpha$ obtained from the dissolution simulations, where γ- is predicted to have an interfacial energy roughly four times larger than either α- or β-glycine. From the interfacial energies, α- and β-glycine nanoparticles were predicted to experience modest solubility increases of up to 1.4 and 1.8 times the bulk solubility, where as γ-glycine showed upward of an 8 times amplification in the solubility. These MD simulations represent a first attempt at a computational (pre)screening method for the rational design of experiments for future engineering of nanocrystal API formulations.

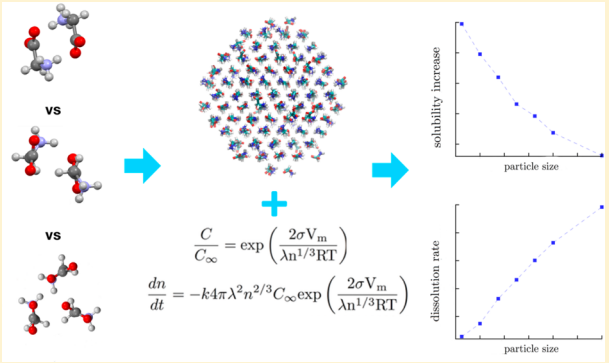


**KEYWORDS:** *molecular dynamics simulation, nanocrystal, polymorph, solubility, bioavailability, dissolution rate*

## INTRODUCTION

For orally administered solid-state active pharmaceutical ingredients (API), the bioavailability is defined as the amount of dissolved API in the blood within a predetermined therapeutic range integrated over time. This API property is one of the most essential design variables of any solid state API crystal, as the bioavailability determines the rate and extent to which the drug becomes available in circulation and hence to what degree the drug can be efficacious. The first step in transferring the drug from the ingested solid state tablet to the bloodstream is the dissolution of the tablet itself, driven by the solubility and area for mass transfer of the solid state tablet. Insufficient dissolution, and hence reduced bioavailability, can result in an inadequate amount of drug being transported to the target, resulting in suboptimal treatment for the patient. Specifically, the API's solubility and dissolution rate must be balanced with its absorption or metabolism rate in order to provide maximum bioavailability. Currently, the pharmaceutical industry is facing a bioavailability crisis, where it is estimated that as high as 60% of newly discovered APIs possess poor aqueous solubility,[1,2] and hence insufficient bioavailability, bringing this problem to the forefront of API manufacturing. Due to the enhanced solubility of the nanocrystal resulting from an increased surface area to volume ratio relative to its micron-sized counterpart, nanocrystal APIs offers an intriguing method to possibly combat poorly soluble bulk crystals. To date, crystal production methods ranging from top down, such as milling or high-pressure homogenizers, to bottom up, such as nanoscale confinement or nanodroplet crystallization, are employed to achieve nanocrystal API product.[3−9] Accelerated dissolution kinetics has been demonstrated upon nanosizing for many poorly aqueous soluble API molecules[10] such as indomethacin,[11] celocoxib,[12] quercetin,[13] ibuprofen,[14] meloxicam,[15] itraconazole,[16] and albendazole.[17] However, no computational framework exists for the screening on nanocrystal polymorphs. Molecular level understanding into the nanocrystal dissolution kinetics as a function of particle size and

**Received:** September 30, 2016
**Revised:** February 13, 2017
**Accepted:** February 21, 2017
**Published:** March 8, 2017






DOI: 10.1021/acs.molpharmaceut.6b00882
*Mol. Pharmaceutics* 2017, 14, 1023−1032

polymorphic form would provide an important step toward designing for optimal nanocrystal drug delivery.

The solubility increase of nanocrystals has its origins in interfacial effects resulting from the large surface area to volume ratio of nanocrystals. Mathematically, this physics is encapsulated in the Ostwald−Freundlich equation for spherical particles, shown below in eq 1:

$$C_e(r) = C_\infty \exp\left(\frac{2\sigma V_m}{rRT}\right) \quad (1)$$

where $r$ is the particle radius, $\sigma$ is the interfacial free energy averaged over all the faces of the crystal exposed to solution, $V_m$ is the molar volume (molecular weight divided by density), $R$ is the gas constant, $T$ is the temperature, $C_\infty$ is the bulk solubility, and $C_e(r)$ is the solubility of the nanoparticle evaluated at particle radius $r$. In addition to the solubility, the dissolution rate is also intimately coupled to the interfacial area for mass transfer, as the net rate of change of solid particle mass is the flux of particles from the surface multiplied by the surface area. Thus, the net effect of nanosizing, specifically whether the dissolution kinetics increase or decrease, will be determined by the competing factors of surface area decrease and solubility increase. As the objective of nanocrystal API manufacturing is to create API tablets with high bioavailability, and not solely solubility, it is critical to determine how the dissolution rate varies with particle size for each solid-state form, as it is not guaranteed that merely reducing the size of the crystal will result in enhanced bioavailability. If a nanocrystal of a given polymorph lies in a surface reaction mass transfer limited regime, a subsequent decrease in the particle size will decrease the dissolution rate due to the decreased surface area. For particles in a diffusion limited mass transfer regime, if the solubility increase does not sufficiently offset the decrease in surface area, the dissolution rate may decrease monotonically with size. Being able to computationally screen to determine how the dissolution rate varies with particle size will allow for the discovery of high bioavailability API products.

Polymorphism is defined as the ability of a molecule to self-assemble into multiple crystalline forms. It is essential to understand that interfacial free energy, $\sigma$ in eq 1, is a polymorph specific parameter for a given solute−solvent liquid composition. Consequently, different crystal structures of the same API molecule will experience different percent increases in the solubility relative to the bulk value in a given solvent. As important, eq 1 implies that the polymorph solubility rankings at bulk length scales need not apply for nanoparticles, a phenomenon known as size dependent polymorphism.[5,7,8] Hence, the stable form obtained under bulk crystallization conditions may potentially become the metastable form upon nanosizing, potentially leading to a reversal in the polymorph dissolution kinetics ranking at the nanoscale when compared to the bulk scale. As key API physical characteristics, such as bioavailability, solid-state stability, and dissolution rate are strong functions of the polymorphic form, it is essential to understand the effects of nanosizing on the polymorphic forms of the target API molecule to choose the appropriate crystal structure for the desired application.[18]

Molecular dynamics (MD) is a simulation methodology in which the positions and velocities of atoms are time integrated forward by solving Newton's equations of motion. With continuous improvements in CPU clock speeds and development of many core architectures such as NVIDIAs graphical processing unit (GPU)[19−21] and the Intel Xeon Phi coprocessor,[22−24] MD has been increasingly applied to study nucleation[25−31] and crystal growth[32−37] of organic crystals. However, the study of organic crystal dissolution using MD has received far less attention. To date, most emphasis has been placed on identifying the dissolution mechanism, and little attention to the size and polymorph dependent dissolution kinetics has been given. Hence, no computational strategy to screen bioavailability with regard to particle size has been proposed. Gao and Olsen identified the dissolution mechanism of acetaminophen form I in water and showed that molecules at edges and corners of a crystal surface detach most readily, due to a decreased interaction with interior crystal molecules.[38] This shows the importance of the interfacial free energy upon dissolution of nanocrystals. The nonspherical seed crystal geometry considered in the work of Gao and Olsen led to an anisotropic distribution of interfacial free energy over the solid molecules on the crystal surface, where molecules on the corners and edge possessed the highest energy, making them dissolve most rapidly. Gao and Olsen later considered the dissolution of form I and form II of acetaminophen for the purpose of identifying solid-state conversion mechanisms.[39] However, only one particle size was considered, and no attempt at quantifying dissolution kinetics was made. Lanaro and Patey performed simulations of NaCl dissolution for various initial crystal shapes (cube, sphere, rod tablet) and identified the dissolution mechanisms.[40] Activation energies were also determined by performing simulations at multiple temperatures. Comparisons with particle size independent classical mass transfer models were performed to determine dissolution kinetics. It was shown that NaCl dissolution is determined mainly by the surface reactivity at the conditions studied. The effect of various particle sizes and the enhancement of the dissolution rate relative to micron sized particles were not considered. Both MD and kinetic Monte Carlo have been used to study the dissolution of aspirin, in which the face specific dissolution kinetics of the experimental morphology were calculated.[41,42] The emphasis of the aspirin works was face specific dissolution kinetics and not on the impact of the size of the particle or the polymorphic form. The dissolution of aspirin, paracetamol, and ibuprofen bulk crystals have also been simulated using MD with the CHARMM, OPLS, and GAFF molecular force fields to evaluate the ability of these force fields to simulate crystal dissolution.[43] However, the dissolution kinetics were not addressed.

In the present work, a computational methodology for the screening of polymorphic nanocrystals for dissolution rate and bioavailability optimization is proposed. Specifically, $\alpha$-, $\beta$-, and $\gamma$-glycine polymorph dissolution kinetics are calculated as a function of particle size through a combination of a parametric mass transfer model and molecular dynamics. Glycine was chosen as a model system as it is an organic molecule that is well parametrized with existing molecular force fields and is known to display size dependent polymorphism.[5,8] The effects of particle size dependent solubility and dissolution kinetics are investigated for each polymorph. The remainder of the article is divided into three parts. In the experimental section, the computational details of the molecular dynamics simulations performed are discussed, and the parametric mass transfer model used is derived. In the results section, the findings of the work are presented. Finally, the main conclusions are summarized in the discussion and conclusion sections.



DOI: 10.1021/acs.molpharmaceut.6b00882
Mol. Pharmaceutics 2017, 14, 1023−1032

## EXPERIMENTAL SECTION

**Dissolution Model.** In this work, the mechanics of dissolution are described using a classical mass transfer model combined with the Ostwald–Freundlich equation. This is necessary as tradition mass transfer models, such as the 1/3 or 2/3 root law, are derived under the case that the solubility of the dissolving particle is not a function of the particle size itself.[44] This is clearly not the case for nanoparticles, as shown by eq 1. Specifically, a Hixson–Crowell type of dissolution equation was employed to model mass transfer. In the Hixson–Crowell equation, the rate at which a substance dissolves is proportional to the exposed solid–liquid surface area, and the difference between the solute concentration in the bulk liquid and the solute concentration at equilibrium.[44] As MD simulations employed in this work track the number of molecules in the dissolving nanocrystal, differential equations in this work will be cast in $(t,n)$ coordinates through the coordinate transformation $r = \lambda n^{1/3}$, where $\lambda$ is a shape factor that converts $n^{1/3}$ to $r$. In these coordinates, the dissolution of a solid particle can be represented by eq 2.

$$\frac{dn}{dt} = k4\pi\lambda^2 n^{2/3}(C_b - C_e) \tag{2}$$

where $n$ is the number of molecules in the dissolving solid at time $t$, $k$ is a constant of proportionality encapsulating resistance to mass transfer in the diffusion layer and interface, $C_b$ is the concentration of dissolved solute, and $C_e$ is the equilibrium solubility of the particle. For particles whose interfacial free energy contributes negligibly to the total free energy of the crystal, $C_e$ is a constant, and the $(r,t)$ version of eq 2 can be integrated to yield the well-known cube-root law. However, for the particle sizes considered in this work, where the initial radius is between 1.85 and 3 nm, the solubility will deviate significantly from bulk solubility values, due to interfacial free energy contributions. Thus, eq 1 is inserted into eq 2 to yield eq 3, the differential equation for dissolution of spherical nanoparticles.

$$\frac{dn}{dt} = k4\pi\lambda^2 n^{2/3}\left(C_b - C_\infty \exp\left(\frac{2\sigma V_m}{\lambda n^{1/3} RT}\right)\right) \tag{3}$$

In the performed simulations, sink conditions for dissolution exist, and hence, $C_b$ is assumed to be zero. Equation 3, therefore, is simplified to yield eq 4.

$$\frac{dn}{dt} = -kC_\infty 4\pi\lambda^2 n^{2/3} \exp\left(\frac{2\sigma V_m}{\lambda n^{1/3} RT}\right) \tag{4}$$

Equation 4 can be expressed as a two-parameter model:

$$\frac{dn}{dt} = -A_1 n^{2/3} \exp\left(\frac{A_2}{n^{1/3}}\right) \tag{5}$$

where the $A_1$ parameter is given by eq 6

$$A_1 = kC_\infty 4\pi\lambda^2 \tag{6}$$

and $A_2$ parameter is given by eq 7

$$A_2 = \frac{2\sigma V_m}{\lambda RT} \tag{7}$$

Finally, the solubility enhancement ratio, for a specified crystal size, is trivially calculated with the knowledge of the $A_2$ parameter and is given by eq 8

$$\frac{C_e(r)}{C_\infty} = \exp\left(\frac{A_2}{n^{1/3}}\right) \tag{8}$$

In this work, the $A_2$ parameter is determined through solid state, liquid, and solid–liquid mixture enthalpy calculations and is discussed in the Enthalpy Balance for Interfacial Energy Calculation section. With knowledge of the polymorph specific $A_2$ parameter, the $A_1$ parameter can simply be regressed to a dissolution trajectory, allowing the calculation of the dissolution rate for any particle size through eq 5.

The dissolution kinetics of polymorphs will be calculated using the Hixson–Crowell model. Although the $C_b - C_e$ driving force for dissolution may not be the correct driving force for particles under surface reaction limitations, it is important to note that the conclusions stated herein are not impacted. As eq 5 is derived to be parametric in form, the ability to screen polymorphs and calculate dissolution kinetics is merely reflected in the quality of fit of the model to the simulated MD data. If a high $R^2$ value is obtained from the fit of eq 5 to the MD dissolution trajectories, the dissolution kinetics can be reliably calculated.

**Enthalpy Balance for Interfacial Energy Calculation.** For the systems considered in this work, which consist of nanocrystals immersed in water, the initial total enthalpy of the system can be decomposed into the terms shown in eq 9 assuming solution ideality:

$$H_{sys} = n_w H_w + n_o H_s + \sigma A \tag{9}$$

where $H_{sys}$ is the total enthalpy of the crystal plus water system, $n_w$ is the total number of water molecules in the MD simulation, $H_w$ is the enthalpy of pure liquid water per water molecule, $n_o$ is the initial number of solid glycine molecules, $H_s$ is the polymorph specific enthalpy per glycine molecule in the bulk solid state (note this is a solid state value and hence contains no interfacial contributions), $\sigma$ is the interfacial energy defined in eq 1, and $A$ is the area of the solid–liquid interface (assumed to be spherical). As three distinct polymorphs are simulated in this study, $H_s$ will have distinct values for $\alpha$-, $\beta$-, and $\gamma$-glycine, represented by the notation $H_\alpha$, $H_\beta$, and $H_\gamma$, respectively. In the case of dissolving crystals, the enthalpy difference between the glycine molecule in the solid and liquid must also be considered, and eq 9 is augmented to yield eq 10:

$$H_{sys}(t) = n_w H_w + n_o H_s + (H_{g,l} - H_s)(n_o - n(t)) + \sigma A \tag{10}$$

where $H_{g,l}$ is the liquid phase glycine enthalpy per glycine molecule, and $n(t)$ is the number of solid glycine molecules at time $t$. It is assumed that $H_{g,l}$ is not a function of any existing dissolved glycine concentration, which is a valid approximation for the low liquid glycine concentrations simulated in this work. To determine the critical polymorph specific $\sigma$ parameter in eq 1 and eq 8, the specific enthalpy values $H_w$, $H_{g,l}$, $H_s$, $H_{sys}(t)$ will be calculated using MD. The details of these calculations are discussed in the Crystal Dissolution and Water Simulation Methods section. Finally, $\sigma$ will be estimated through parameter estimation using $H_{sys}(t)$, $n(t)$, $H_w$, $H_{g,l}$ and $H_s$. The parameter estimation methodology is discussed in the Parameter Estimation section. Once the value of $\sigma$ is known, the $A_2$ parameter in the Hixson–Crowell mass transfer model can be calculated using eq 7. Using the newly calculated value of $A_2$, $A_1$ is regressed to each average dissolution trajectory allowing for dissolution rate calculation through eq 5. Figure 1 provides a pictorial overview of the employed method.



DOI: 10.1021/acs.molpharmaceut.6b00882
Mol. Pharmaceutics 2017, 14, 1023–1032

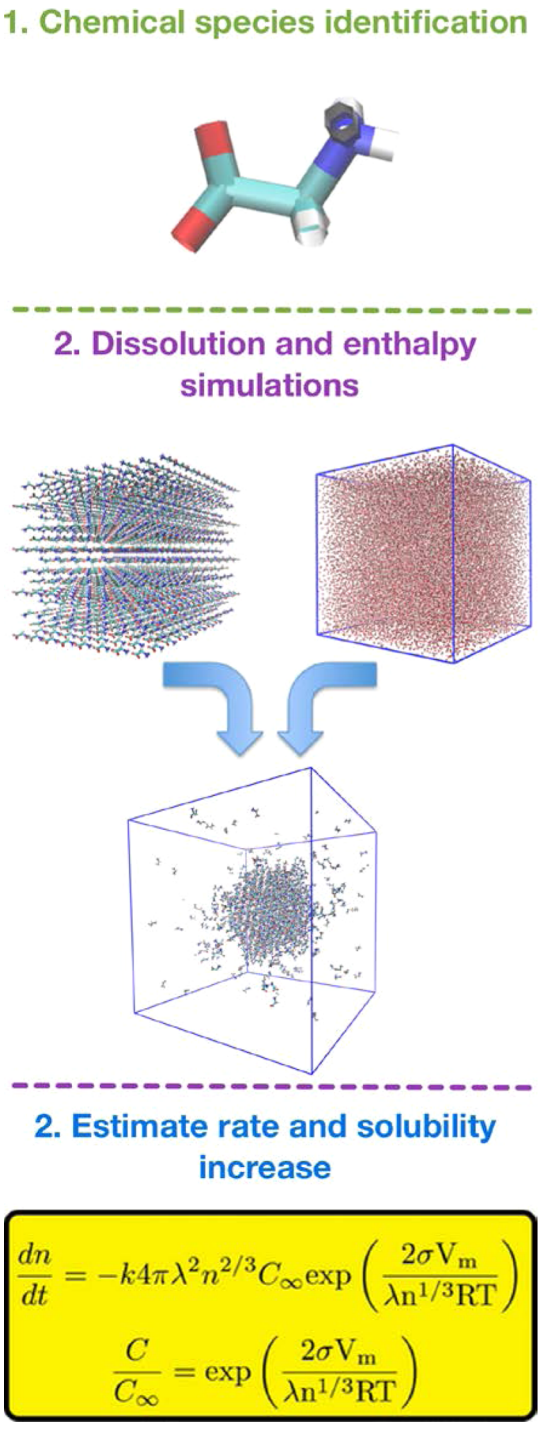


**Figure 1.** Methodology overview. In step 1, the drug molecule is specified. In step 2, bulk solid-state, pure liquid phase, and nanocrystal dissolution simulations are performed. The enthalpy and dissolution trajectories are used to estimate the parameters in step 3 to calculate solubility increase and dissolution kinetics.

It must be remarked that $\sigma$ in eq 1 is technically a free energy. Thus, by equating the interfacial energy in eq 8 with that in eq 1, we are neglecting entropy contributions to the interfacial energy, resulting from the partial ordering of liquid molecules at the surface of the solid crystal. Including the entropy contributions would require more computationally expensive free energy sampling computational procedures[45] and may very well yield a statistically equivalent answer to the enthalpy result for the case of the Zwitter-ion glycine, where molecule−molecule interactions will be dictated heavily by electrostatic potential energy contributions. This has indeed been found to be the case of NaCl, where the interfacial energy using the enthalpy approximation yielded a statistically equivalent estimate of the interfacial free energy generated using more rigorous free energy sampling procedures.[46]

As mentioned in the introduction, the calculated interfacial energy represents the average interfacial energy averaged over all crystal faces exposed to solution during the dissolution process. This estimate needs to be distinguished from face specific bulk crystal−liquid interfacial energy estimates. In addition, previous MD studies have shown nanocrystal interfacial energies may differ significantly from their bulk counter parts due to Tollman-length and surface curvature contributions.[45]

**Crystal Dissolution and Water Simulations.** In all simulations performed, the GAFF force field with CNDO atomic charges was used to simulate glycine. For water, the SPC/E water model was employed.[47] Standard GAFF force field parameter combination rules were used for all simulations.

All crystal dissolution simulations were performed using an in-house MD code suited for embarrassingly parallel multiple replica simulations on Intel Xeon Phi coprocessor hardware.[22] In all simulations, initial trajectories were launched by generating randomly initialized atomic velocities according to a Maxwellian velocity distribution. Short-range nonbonded forces were truncated at 1.2 nm. Reciprocal space electrostatic forces were computed using a particle mesh ewald (PME) solver with a $1 \times 10^{-6}$error tolerance. The number of PME grid points was 100 in each direction. The temperature was controlled using a Langevin thermostat with a relaxation time of 2000 fs. The isotropic Berendsen barostat was used with a 1000 fs relaxation time and a set point of 1 atm for water equilibration and crystal dissolution simulations. A value of 21454.85 atm was used for the bulk modulus of water to determine the relaxation time constant in the Berendsen barostat. The shake algorithm was employed to constrain the motion of all bonds containing hydrogen. A shake tolerance of $1 \times 10^{-4}$ was employed for all simulations, and a maximum number of 25 shake iterations were allowed. Periodic boundary conditions were employed in all directions. For all production runs, the equations of motion were solved using a velocity Verlet algorithm with a 2.0 fs time step.

To prepare an initial configuration of water molecules for crystal dissolution simulations, a 9.5 nm cubic box was solvated with SPC/E water molecules using the gromacs/5.0[48] solvate command. The system was then equilibrated for 6 ns in the NVT ensemble. The system was then equilibrated for an additional 6 ns in the NPT ensemble for a total of 12 ns of equilibration. All equilibration runs were performed at 330 K. The final equilibrated configuration of water molecules was then used to solvate polymorph specific seed crystals of various sizes, again using the gromacs/5.0 solvate command. The energy of the system was minimized in gromacs/5.0, using steepest descent minimization, with an energy minimization tolerance of 100.0 kJ/mol/nm. Polymorph specific seed crystals were obtained by cutting 1.85, 2.0, 2.15, 2.30, 2.45, 2.60, and 3.0 nm radius $\alpha$-, $\beta$-, and $\gamma$-glycine spherical crystals from their respective bulk structures. The selection of these particle sizes allowed a large number of nanocrystal sizes to be simulated while keeping the distance between periodic images larger than three cut-off lengths. This was done to minimize spurious finite


DOI: 10.1021/acs.molpharmaceut.6b00882
Mol. Pharmaceutics 2017, 14, 1023−1032

size effects. Bulk structures for seed generation were obtained from the Cambridge Crystal Structure Database.[49] Ten independent crystal dissolution trajectories were then launched from each initial crystal considered. This allows the averaging of any stochasticity in the dissolution time series profile and allows for the calculation of the average crystal dissolution kinetics. The first 0.1 ns of a crystal dissolution simulation were attributed to equilibration, and data was not monitored during this time. After equilibration, the dissolution dynamics were monitored for 0.5 ns for parameter estimation and data generation. This length of simulation provided ample data for the enthalpy calculations, as well as mass-transfer model parameter estimation, without any significant dissolved glycine concentration accumulating. This validates the sink conditions $C_b = 0$ approximation in the dissolution model development.

To calculate the specific enthalpy of water at the conditions employed in these simulations, the equilibrated SPC/e water box was further propagated in time using MD for an additional 2 ns. The total enthalpy of the system was monitored, and the enthalpy per water molecule was calculated as the average enthalpy over time divided by the total number of water molecules in the simulation. To determine the enthalpy of liquid glycine, the 1.85 nm $\alpha$-glycine crystal was simulated until well past complete dissolution for all 10 trajectories. Specifically, all 10 trajectories were simulated for 7.5 ns. Data was recorded over the final ns. This corresponds roughly to a dissolved glycine concentration of $C_b = 0.05$ g/cm$^3$ or $C_b = 0.4$ glycine molecules/nm$^3$. To simplify the methodology employed here, a potential dependence of the liquid glycine enthalpy on the liquid glycine concentration is neglected. However, $C_b = 0.4$ glycine molecules/nm$^3$ implies that the number of glycine molecules within the 1.2 nm force field cutoff employed is 0.7 glycine molecules on average. Therefore, any potential contribution of glycine−glycine interactions to the liquid glycine enthalpy is not expected to contribute significantly to the liquid glycine enthalpy, as the vast majority of interactions will be glycine−water in nature. The resulting liquid glycine enthalpy was then calculated as the average glycine enthalpy (total enthalpy−water enthalpy) over the final 1 ns time interval, divided by the total number of glycine molecules.

**Clustering Algorithm for Solid Particle Identification.** A local density criterion was used to determine if a glycine molecule was a solid or liquid molecule.[31,40,50] Glycine molecules were considered solid if it possessed 11 or more neighbors in a 0.6 nm radius sphere.[50] That distance roughly corresponds to the first minimum in the glycine−glycine center radial distribution function. This number of neighbors corresponds to the tail end of the bulk glycine density distribution. A clustering algorithm was then employed to determine the instantaneous size of the embedded crystal. Although they do not meet the solid molecule density criterion, it is important to include surface molecules in the clustering algorithm, as they make up an increasingly large percentage of the total number of solid molecules as the crystal size decreases. Surface molecules were included in the clustering algorithm by counting a molecule as solid if it had a neighbor who met the density criterion, but did not meet the density criterion itself.

**Solid State Crystal Lattice Simulations.** For the triclinic box based solid-state calculations of $\alpha$-, $\beta$-, and $\gamma$-glycine, the LAMMPS[51] simulation package was employed. A Nose−Hoover chain with a temperature relaxation time of 2 ps and a pressure relaxation time of 1 ps was implemented for time integration and temperature/pressure control. For all three polymorphs, the crystal lattice was equilibrated at 330 K using the following procedure: (1) energy minimization with an energy and force tolerance of $1 \times 10^{-6}$; (2) NVT equilibration for 2 ns; (3) NPT equilibration for 2 ns using isotropic coupling; (4) NPT equilibration for 2 ns using anisotropic pressure coupling. This was done to allow the pressure and volume to equilibrate before allowing the box lengths to fluctuate independently. Following equilibration, a production run of 2 ns was performed in the NPT ensemble with anisotropic pressure coupling, during which time the system enthalpy was monitored. The glycine solid-state enthalpy was calculated as the average enthalpy over time during the 2 ns production run divided by the number of glycine molecules in the crystal lattice.

**Parameter Estimation.** To determine $\sigma$ for each polymorph, optimization based parameter estimation was employed. Due to the ratio of glycine molecules to water molecules in these simulations, which ranged between 1:100 and 6:100, the small enthalpy contribution of the glycine molecules to the total enthalpy made the parameter estimation sensitive to which data sets were fitted. To prevent a biased estimate of the interfacial energy, we selected four to seven data sets at random, and calculated the average interfacial energy over many iterations. An enthalpy time series data set was selected with probability 0.75, and the sum of squared error between the predicted average enthalpy during dissolution from eq 10 and the enthalpy time series data generated from all the polymorph specific nanocrystal dissolution runs was minimized. This procedure was conducted 1000 times with 1000 different initial parameter guesses. The $\sigma$ value was recorded, and the parameter estimation procedure was employed three additional times. This yields four $\sigma$ values for averaging and statistical uncertainty analysis for a fixed polymorph, and a value for $\sigma$ that best describes the average enthalpy during dissolution for all particle sizes simulated. The final reported $A_2$ value reported is calculated using the average $\sigma$ from all four parameter estimation runs for a given polymorph. To estimate the $A_1$ parameter in eq 5, the MD generated polymorph specific dissolution data, along with the $A_2$ parameter value predetermined from the enthalpy calculations, is used to calculate the best-fit parameter value for each of the seven polymorph specific average dissolution trajectories. To generate trial solutions to eq 5, eq 5 was solved using ode45 in MATLAB, using trial parameter values generated by the optimization algorithm as it iterates toward the best fit solution. Specifically, the resulting sum of squared error between the model prediction and MD data was minimized using fminsearch in MATLAB to yield the optimal parameter values.

## RESULTS

**Interfacial Energy and Solubility Increase.** In Table 1, the specific enthalpy values $H_w$, $H_{g,l}$, $H_\alpha$, $H_\beta$, and $H_\gamma$ are presented.

From the estimated enthalpies, the enthalpy of solvation, $\Delta H_{solv}$, can be calculated from the difference between glycine in solution and in the solid-state. $\Delta H_{solv}$ is predicted to be 12.9 kJ mol$^{-1}$ for $\alpha$- and $\beta$-glycine, and 13.2 kJ mol$^{-1}$ for $\gamma$-glycine.

The values in Table 1 were used in eq 8, and $\sigma$ was subsequently determined for each polymorph through the parameter estimation procedure discussed in the Parameter Estimation section. The time series enthalpy data and model fit is found in Supporting Information, Figure S1. The $\sigma$ values are presented in Table 2.



DOI: 10.1021/acs.molpharmaceut.6b00882
Mol. Pharmaceutics 2017, 14, 1023−1032

Table 1. Calculated Specific Enthalpy Values for $H_w$ (Liquid Water), $H_{g,l}$ (Liquid Glycine), $H_\alpha$ ($\alpha$-Glycine), $H_\beta$ ($\beta$-Glycine), and $H_\gamma$ ($\gamma$-Glycine)

| material variable | enthalpy per molecule (kcal/mol) |
|---|---|
| $H_w$ | $-8.69 \pm 1.87 \times 10^{-4}$ |
| $H_{g,l}$ | $-61.71 \pm 5.38 \times 10^{-2}$ |
| $H_\alpha$ | $-64.79 \pm 0.80$ |
| $H_\beta$ | $-64.76 \pm 0.78$ |
| $H_\gamma$ | $-64.87 \pm 0.67$ |

Table 2. Polymorph Specific $\sigma$ Values for $\alpha$-, $\beta$-, and $\gamma$-Glycine

| polymorph | $\sigma$ (mJ/m$^2$) | $A_2$ |
|---|---|---|
| $\alpha$ | 19.1 ± 0.11 | 2.45 |
| $\beta$ | 31.9 ± 0.27 | 4.10 |
| $\gamma$ | 112.8 ± 0.51 | 14.53 |

Equipped with the knowledge of $\sigma$ and the $A_2$ parameter for each polymorph, the multiplicative increase in solubility can be calculated for each of the initial particle sizes simulated in this work. The results are shown in Figure 2.

**Polymorph Specific Dissolution Kinetics.** With the data generated from MD for each polymorph and crystal size, and the $A_2$ parameter results in Table 2, the remaining $A_1$ parameter in eq 5 is regressed for each averaged dissolution trajectory. This results in a high degree of model fit to the dissolution data, above $r^2 = 0.95$ for all data sets, allowing for an accurate calculation of the dissolution kinetics. As an example, the dissolution data and model fit for the 3 nm $\alpha$-, $\beta$-, and $\gamma$-polymorphs are shown in Figure 3A. All dissolution trajectories can be found in the Supporting Information, Figure S2, along with the associated model fits. In Figure 3B, we plot the $A_1$ parameter for every initial particle size simulated, for all three polymorphs simulated in this work. Finally, knowledge of the polymorph specific dissolution model parameters in eq 5 allows for the calculation of polymorph specific dissolution rates. The dissolution rate calculated at the initial particle size (before dissolution trajectory equilibration) for each polymorph is plotted in Figure 4.

## DISCUSSION

From the solid-state enthalpy calculations obtained for each polymorph, the difference in crystal lattice stabilities are found to be minimal at 330 K. This is in line with crystal structure prediction results, which show that $\gamma$-glycine is the global minimum in lattice energy by only a few $kT$.[52−54] The calculated value of $\Delta H_{solv}$ agrees well with the 17.3 kJ mol$^{-1}$ $\alpha$-glycine experimental value calculated from the van't Hoff equation.[31,55] This is also in agreement with previous estimates from our group[31] of 10.64 kJ mol$^{-1}$, but is above the 3.1 kJ mol$^{-1}$ value predicted by Cheong and Boon.[47] However, the Cheong and Boon value was predicted at 298 K, which could explain their lower value. Although the bulk lattices are predicted to be similar in stability from the enthalpies, this is shown to not be the case upon the insertion of the different polymorphs of glycine into water. In solution, the inability of $\gamma$-glycine to form energetically favorable configuration with the aqueous medium render it much more unstable than either $\alpha$-glycine or $\beta$-glycine. This highlights the drastic effects that solvents can play on the stability and kinetics of polymorphs. Specifically, $\gamma$-glycine is shown to possess the largest $\sigma$ (112.8 mJ/m$^2$) by a factor of 3−6 relative to $\alpha$- (19.1 mJ/m$^2$) and $\beta$-glycine (31.9 mJ/m$^2$). Due to the magnitude of the $\gamma$-glycine interfacial energy with water; $\gamma$ is predicted to have a much larger solubility increase upon nanosizing according to eq 1. Whereas $\alpha$- and $\beta$-glycine are shown to only possess a 1.25−1.42 and 1.44−1.81 magnification in solubility respectively, $\gamma$-glycine is shown to possess a 3.63−7.95 times increase in the solubility. This makes $\gamma$-glycine potentially the attractive polymorphic form for a glycine nanocrystal application in vivo. Finally, for all polymorphs, the enthalpy of glycine in the liquid is predicted to be higher than that in the solid state. This shows that the dissolution of these nanocrystals is driven by the entropy difference between glycine in the liquid and glycine in the solid.

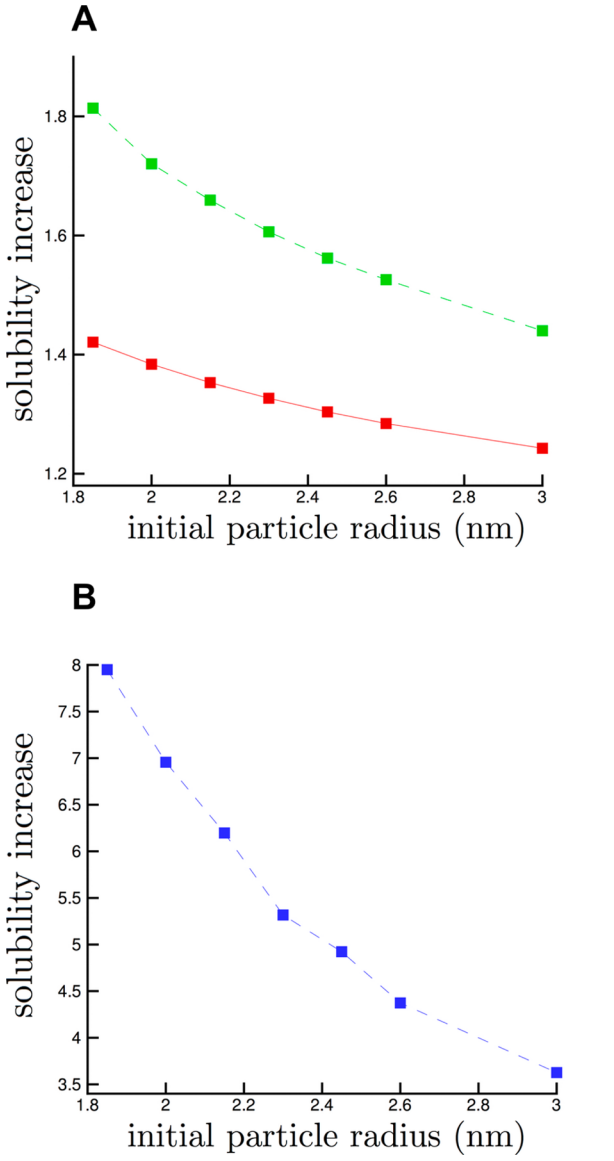


**Figure 2.** Multiplicative increase in the nanocrystal solubility relative to the bulk value for (A) $\alpha$- (red), $\beta$- (green), and (B) $\gamma$-glycine (dark blue) nanocrystals.

Although the exact $\beta$-glycine bulk solubility value is not measurable in water due to rapid recrystallization kinetics,[56] the experimentally measured bulk solubility values of $\alpha$- and $\gamma$-glycine are statistically equivalent at 330 K, with $\alpha$-solubility reported as 38.5 ± 1.5 g/kg water at 55 °C, and $\gamma$- solubility


DOI: 10.1021/acs.molpharmaceut.6b00882
Mol. Pharmaceutics 2017, 14, 1023−1032

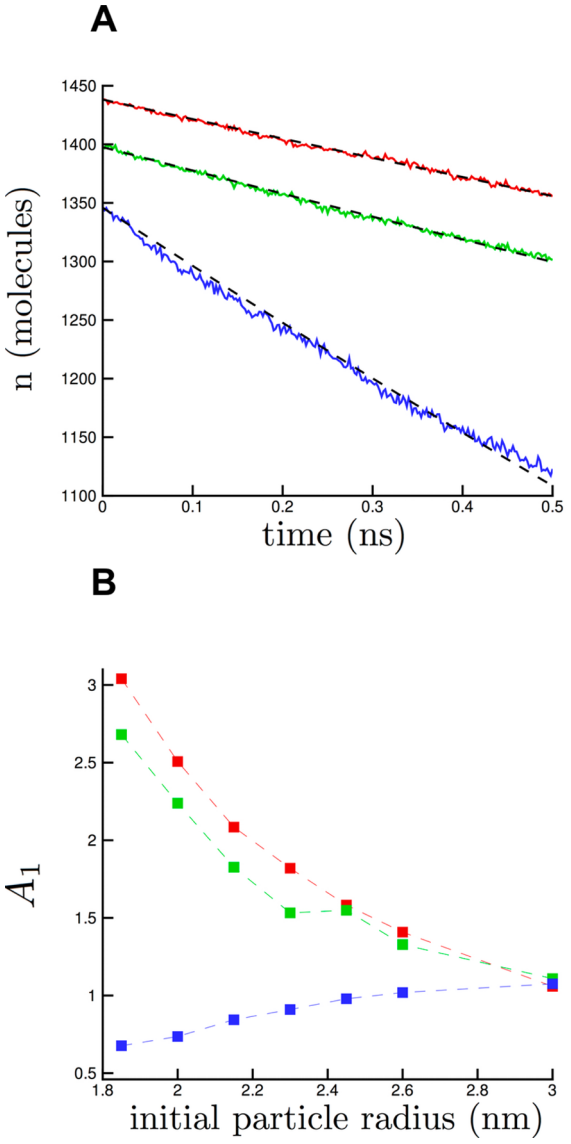


**Figure 3.** (A) Average dissolution trajectories, along with associated model fit (dashed black line), are plotted for the 3 nm $\alpha$- (red), $\beta$- (green), and $\gamma$- (dark blue) nanocrystals. (B) Estimated $A_1$ parameter for all $\alpha$- (red), $\beta$- (green), and $\gamma$-glycine (dark blue) nanocrystals vs initial particle size (nm).

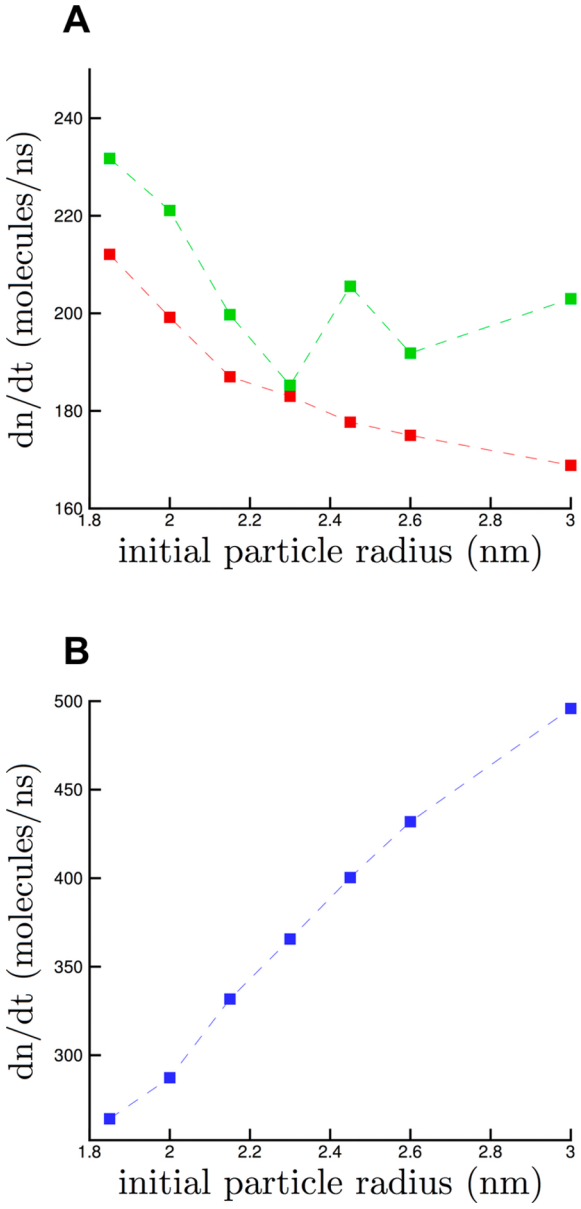


**Figure 4.** Calculated dissolution rate (molecules/ns) vs initial particle size (nm) for all $\alpha$- (red), $\beta$- (green), and $\gamma$-glycine (dark blue) nanocrystals.

reported as 37.6 ± 1.6 at 57 °C, making the polymorph stability ranking $\alpha$- ≈ $\gamma$-glycine > $\beta$-glycine.[55] Using the solubility increase values reported in this work, $\gamma$-glycine solubility would range between 299 g/kg water for the 1.85 nm particle and 136 g/kg water for the 3.0 nm particle. With its modest $\sigma$ value of 19.1 mJ/m$^2$, $\alpha$-glycine solubility would range between 47.7 and 54.7 g/kg water, much lower than that of $\gamma$-glycine nanocrystals of equivalent size. This yields the polymorph stability ranking $\alpha$- > $\gamma$-glycine at the nanoscale. This result is in agreement with previous nucleation simulation of glycine in aqueous solution performed by our group at supersaturated concentrations, where the melting temperature of $\gamma$-glycine nanocrystals was up to 20 K below $\alpha$-glycine nanocrystals.[31] This shows how bulk scale material knowledge is poorly transferred to the nanoscale, where new physics, emanating from the enhanced surface area to volume ratio of the particles, dictates the stability, solubility, and dissolution kinetics. Our recent MD nucleation simulations at supersaturated and lower temperature conditions have predicted a lower $\sigma$ value for $\beta$-glycine (17.97 mJ/m$^2$) than $\alpha$-glycine (31.0 mJ/m$^2$).[31] This suggests that the $\sigma$ rankings may undergo a reversal as a function of the liquid glycine concentration. This could result in different glycine polymorphs nucleating as a function of the applied supersaturation.

Upon batch crystallization from aqueous solution, the $\alpha$-glycine polymorph is commonly produced.[57] However, $\gamma$-glycine is the most stable lattice, posing the question as to why $\gamma$ is not obtained from aqueous crystallization. From a classical nucleation theory perspective, which views the crystallization process as a competition between the energetically favored formation of the new solid phase, and the energetically unfavorable creation of an interface, these $\sigma$ results potentially rationalize why $\gamma$-glycine, despite being the thermodynamically preferred crystal lattice, is not observed upon batch crystallization in aqueous solution, but rather $\alpha$-glycine. From the experimentally determined solubility values[55,56] of the three


DOI: 10.1021/acs.molpharmaceut.6b00882
*Mol. Pharmaceutics* 2017, 14, 1023−1032

polymorphs, γ-glycine would have a chemical potential difference between the metastable liquid and solid similar to α-glycine, and even greater than β-glycine. However, the large σ value would render the free energy barrier to nucleation largest for γ-glycine and render the kinetic accessibility of γ-glycine negligible. This is equivalent to the results found in our previous MD nucleation study.[31]

There is an observed direct correlation between the magnitude of σ of a polymorph and the rate of dissolution, with the rate of dissolution ranking, $\gamma > \beta > \alpha$, being the same as the σ ranking. However, solubility increase alone need not guarantee that the dissolution kinetics increase with decreasing cluster size. Of the three polymorphs studied in this work, only α-glycine, the polymorph with the lowest σ, is observed to display a monotonic increase in the dissolution rate with decreasing particle size. In the case of α-glycine, the dissolution kinetics are observed to vary from 212 molecules/ns in the 1.85 nm particle case, to the lowest dissolution rate of 169 molecules/ns obtained with the 3 nm α-glycine cluster, a roughly 20% decrease in the dissolution rate. β-Glycine dissolution kinetics display a unique minimum in the dissolution rate, where the dissolution rate increases as the size is increased past 2.3 nm, and this dissolution rate increases as the size decreases past 2.3 nm. For the β-glycine nanocrystal of these sizes, the competing effects of surface area and solubility increase are of equal magnitude, leading the unique minimum in the observed dissolution rate of the range of particle sizes. Although glycine is known to display size dependent polymorphism at supersaturated conditions,[8] we predict β-glycine nanocrystals to dissolve at rates greater than or equal to α-glycine for all particle sizes tested. γ-Glycine nanocrystals display the opposite dissolution kinetics trend to α-. It is shown that the dissolution kinetics of γ-glycine decreases monotonically with decreasing particle size, despite γ-glycine possessing the highest σ of any of the polymorphs. It is likely that the high driving force for diffusive mass transfer, $C_b - C_e(r)$, has rendered the rate of molecular detachment from the solid cluster the rate limiting step of the dissolution process. As the number of molecular detachments would scale proportionally with the surface area, this would rationalize the qualitative trend in the dissolution kinetics of γ-glycine. Since the dissolution rate as a function of particle size and, in turn, time, ultimately dictates the amount of available drugs in the body, our finding highlights the fact that the solubility increase of a nanoparticle due to size reduction need not guarantee an increase in the API bioavailability. From the data generated for each polymorphic form, and if the primary concern is the maximize the dissolution rate of the dissolving glycine crystal, γ-glycine would be the form predicted by our simulations.

Administered nanoparticle API tablets are frequently biphasic systems consisting of nanosize drug particles formulated with stabilizing surfactants.[10] Surfactants are needed to prevent agglomeration of nanoparticles seeking to reduce their surface area to volume ratio. The nanocrystal dissolution rate has also been shown to be a function of the stabilizing surfactant molecule employed.[16] This could prevent the current set of simulation data from agreeing with future measurements of the dissolution kinetics of glycine nanocrystals formulated with a stabilizing surfactant, as the impact of different formulations is not addressed in this work. Future MD computational work will seek to screen surfactants in addition to polymorphic type, although large surfactant molecules could present a significant computational challenge. Currently, particle size distributions of nanocrystals commonly have average particle sizes ranging between 200 and 600 nm using conventional top down preparation procedures such as such as milling or high-pressure homogenizers.[58] These particle sizes are 2 orders of magnitude larger than what MD can currently simulate. However, MD can simulate the smallest particle sizes produced by bottom-up nanocrystal production approaches. As such, the dissolution kinetics of nanocrystals produced using these bottom up approaches could be directly compared against MD simulations. Bottom up nanoscale crystallization methods have produced nanocrystals between 5 and 100 nm in diameter, although these methods are not currently sufficiently scalable to be used for manufacturing.[5,7−9] As the aforementioned issues are solely barriers through the computational time required to simulate 200 nm particles and various stabilizing surfactant molecules, we believe the method in general will extend to more complicated organic molecules and formulations, and therefore, the results presented herein present a first attempt at a computationally prescreening for future engineering of nanocrystal API formulations.

## CONCLUSION

As an increasingly large fraction of newly discovered API candidates are shown to possess poor aqueous solubility, and hence potential bioavailability, nanocrystals are receiving increasing attention due to their enhanced solubility relative to their micron sized counterpart. The physical origin of this solubility increase with nanosizing, the interfacial free energy σ between the crystal and the aqueous medium is a polymorph specific parameter, creating an additional material property for consideration when selecting which solid state form is appropriate for the desired application. Furthermore, as the nanocrystal stability upon size reduction will be determined increasingly by the magnitude of σ, the nanocrystal stability ranking (solubility) need not be the same as that which was determined at the micron scale.

MD provides a simulation methodology in which the dissolution trajectories of organic crystals can be monitored with femtosecond resolution and fully atomistic detail. However, to date, only limited attention has been paid to the problem of determining nanocrystal dissolution kinetics or solubility increase, with the bulk of pharmaceutical based MD simulations being devoted to the equally pressing problems of crystal growth and nucleation. In this work, the dissolution trajectories of the three experimentally observed polymorphs of glycine (at atmospheric conditions), α-, β-, and γ-glycine, were studied to determine the effects of the polymorphic form on the resulting dissolution kinetics and solubility increase. Through an analysis of the enthalpy time-series data generated during dissolution, estimates for the interfacial energy for all polymorphs were calculated.

Using the outlined methodology, it is shown that γ-glycine has an interfacial energy (112.8 $mJ/m^2$) roughly 3−6 times larger than either α- (19.1 $mJ/m^2$) or β-glycine (31.9 $mJ/m^2$) at sink conditions (no dissolved glycine). Using the Ostwald−Freundlich equation, the resulting multiplicative solubility increases, relative to the bulk crystal value, over the range of cluster sizes simulated in this work, were 1.25−1.42 for α-glycine, 1.44−1.81 for β-glycine, and 3.63−7.95 for γ-glycine. A Hixson-Crowell type dissolution model, augmented with the Ostwald−Freundlich equation, was then employed to calculate the dissolution kinetics for each initial particle size and


DOI: 10.1021/acs.molpharmaceut.6b00882
Mol. Pharmaceutics 2017, 14, 1023−1032

polymorph. Of the three polymorphs, only the dissolution kinetics of $\alpha$-glycine is observed to decrease monotonically with increasing cluster size. On the contrary, $\gamma$-glycine is shown to exist in the surface area limited regime, where the dissolution kinetics increases monotonically with increasing cluster size. The physical rationale for the surface area limited regime proposed in this work is that the large interfacial energy of $\gamma$-glycine makes the driving force for diffusion, the concentration gradient between the bulk and the solubility, so large that the limiting rate becomes molecular detachment at the interface. The large interfacial energy of $\gamma$-glycine, relative to its polymorph counterparts, results in the dissolution kinetics of $\gamma$-glycine being 1.5−2× larger than either $\alpha$- or $\beta$-glycine. Finally, $\beta$-glycine is predicted to exist in an intermediate regime, where the dissolution kinetics shows a distinct local minimum over the range of cluster sizes studied. It is worthwhile to note that, in this work, the topic of solid-state polymorphic transformation has not been addressed. Given our latest finding, this issue becomes even more important when tuning bioavailability at the nanoscale since the rate of dissolution will dramatically change if unforeseen transformation takes place. This is a subject of future work. Also, thus far, sufficiently accurate, sensitive, and reproducible methods needed to determine bioavailability have solely been experimental, i.e., *in vitro* or *in vivo* methods. These MD simulations represent a first attempt at computational (pre)screening method for rational design of experiments for future engineering of nanocrystal API formulations.

## ■ ASSOCIATED CONTENT

### Supporting Information

The Supporting Information is available free of charge on the ACS Publications website at DOI: 10.1021/acs.molpharmaceut.6b00882.

Figures of dissolution enthalpies and number of solid molecules vs time (PDF)

## ■ AUTHOR INFORMATION


### Corresponding Author

*E-mail: ramkrish@ecn.purdue.edu.

### ORCID

Doraiswami Ramkrishna: 0000-0001-8158-5116

### Present Address

§(H.-H.T.) School of Chemical Engineering, Purdue University, 480 West Stadium Mall, West Lafayette, Indiana 47907, United States


### Author Contributions

The manuscript was written through contributions of all authors. All authors have given approval to the final version of the manuscript.

### Notes

The authors declare no competing financial interest.

## ■ ACKNOWLEDGMENTS

This study was sponsored by AbbVie Inc. This work used the Extreme Science and Engineering Discovery Environment (XSEDE), which is supported by National Science Foundation grant number ACI-1053575. This work used the XSEDE Extended Collaborative Support Service (ECSS) program. The authors would like to acknowledge XSEDE and Purdue RCAC, as all simulations were performed on Stampede supercomputer at TACC and Conte supercomputer at Purdue. The authors were given access to Stampede supercomputer through XSEDE grant CHE150072. The authors would like to acknowledge the tremendous help provided by Lei Huang and Yang Wang at TACC and Xiao Zhu for their assistance in parallelizing the MD platform on Stampede and Conte. This study was sponsored by AbbVie Inc. through grant number 8000053025 and 8000069224. Hsien-Hsin Tung was AbbVie employee at the time that he collaborated on this project. Nandkishor Nere and Shailendra Bordawekar are present employees of AbbVie Inc.

## ■ REFERENCES


(1) Junghanns, J.-U. A. H.; Müller, R. H. Nanocrystal Technology, Drug Delivery and Clinical Applications. *Int. J. Nanomed.* **2008**, *3* (3), 295−309.

(2) Hasa, D. Drug Nanocrystals: Theoretical Background of Solubility Increase and Dissolution Rate Enhancement. *Chem. Biochem. Eng. Q.* **2014**, *28* (3), 247−258.

(3) Keck, C. M.; Müller, R. H. Drug Nanocrystals of Poorly Soluble Drugs Produced by High Pressure Homogenisation. *Eur. J. Pharm. Biopharm.* **2006**, *62* (1), 3−16.

(4) Rabinow, B. E. Nanosuspensions in Drug Delivery. *Nat. Rev. Drug Discovery* **2004**, *3* (9), 785−796.

(5) Jiang, Q.; Ward, M. D. Crystallization under Nanoscale Confinement. *Chem. Soc. Rev.* **2014**, *43* (7), 2066−2079.

(6) Kim, K.; Lee, I. S.; Centrone, A.; Hatton, T. A.; Myerson, A. S. Formation of Nanosized Organic Molecular Crystals on Engineered Surfaces. *J. Am. Chem. Soc.* **2009**, *131* (51), 18212−18213.

(7) Hamilton, B. D.; Ha, J.; Hillmyer, M. A.; Ward, M. D. Manipulating Crystal Growth and Polymorphism by Confinement in Nanoscale Crystallization Chambers. *Acc. Chem. Res.* **2012**, *45* (3), 414−423.

(8) Hamilton, B. D.; Hillmyer, M. A.; Ward, M. D. Glycine Polymorphism in Nanoscale Crystallization Chambers. *Cryst. Growth Des.* **2008**, *8* (9), 3368−3375.

(9) Rengarajan, G. T.; Enke, D.; Beiner, M. Crystallization Behavior of Acetaminophen in Nanopores. *Open Phys. Chem. J.* **2007**, *1*, 18−24.

(10) Dizaj, S. M.; Vazifehasl, Z.; Salatin, S.; Adibkia, K.; Javadzadeh, Y. Nanosizing of Drugs: Effect on Dissolution Rate. *Res. Pharm. Sci.* **2015**, *10* (2), 95−108.

(11) Rezaei Mokarram, a; Kebriaee Zadeh, A.; Keshavarz, M.; Ahmadi, A.; Mohtat, B. Preparation and in-Vitro Evaluation of Indomethacin Nanoparticles. *Daru* **2010**, *18* (3), 185−192.

(12) Liu, Y.; Sun, C.; Hao, Y.; Jiang, T.; Zheng, L.; Wang, S. Mechanism of Dissolution Enhancement and Bioavailability of Poorly Water Soluble Celecoxib by Preparing Stable Amorphous Nanoparticles. *J. Pharm. Pharm. Sci.* **2010**, *13* (4), 589−606.

(13) Kakran, M.; Sahoo, N. G.; Li, L. Dissolution Enhancement of Quercetin through Nanofabrication, Complexation, and Solid Dispersion. *Colloids Surf., B* **2011**, *88* (1), 121−130.

(14) Mansouri, M. Preparation and Characterization of Ibuprofen Nanoparticles by Using Solvent/ Antisolvent Precipitation. *Open Conf. Proc. J.* **2011**, *2* (1), 88−94.

(15) Raval, A. J.; Patel, M. M. Preparation and Characterization of Nanoparticles for Solubility and Dissolution Rate Enhancement of Meloxicam. *Int. Res. J. Pharm.* **2011**, *1* (2), 42−49.

(16) Badawi, A. A.; El-Nabarawi, M. A.; El-Setouhy, D. A.; Alsammit, S. A. Formulation and Stability Testing of Itraconazole Crystalline Nanoparticles. *AAPS PharmSciTech* **2011**, *12* (3), 811−820.

(17) Koradia, Dk.; Parikh, Hr. Dissolution Enhancement of Albendazole through Nanocrystal Formulation. *J. Pharm. BioAllied Sci.* **2012**, *4* (5), 62.

(18) Lee, A. Y.; Erdemir, D.; Myerson, A. S. Crystal Polymorphism in Chemical Process Development. *Annu. Rev. Chem. Biomol. Eng.* **2011**, *2*, 259−280.

(19) Goetz, A. W.; Williamson, M. J.; Xu, D.; Poole, D.; Le Grand, S.; Walker, R. C. Routine Microsecond Molecular Dynamics Simulations

with Amber - Part I: Generalized Born. *J. Chem. Theory Comput.* **2012**, *8*, 1542−1555.
(20) Anderson, J. A.; Lorenz, C. D.; Travesset, A. General Purpose Molecular Dynamics Simulations Fully Implemented on Graphics Processing Units. *J. Comput. Phys.* **2008**, *227* (10), 5342−5359.
(21) Le Grand, S.; Götz, A. W.; Walker, R. C. SPFP: Speed without Compromise - A Mixed Precision Model for GPU Accelerated Molecular Dynamics Simulations. *Comput. Phys. Commun.* **2013**, *184* (2), 374−380.
(22) Parks, C.; Huang, L.; Wang, Y.; Ramkrishna, D. Accelerating Multiple Replica Molecular Dynamics Simulations Using the Intel® Xeon Phi Coprocessor. *Mol. Simul.* **2016**, DOI: 10.1080/08927022.2017.1301666. Accepted.
(23) Pennycook, S. J.; Hughes, C. J.; Smelyanskiy, M.; Jarvis, S. A. Exploring SIMD for Molecular Dynamics, Using Intel® Xeon® Processors and Intel® Xeon Phi Coprocessors. In *2013 IEEE 27th International Symposium on Parallel and Distributed Processing*; IEEE, 2013; pp 1085−1097.
(24) Needham, P. J.; Bhuiyan, A.; Walker, R. C. Extension of the AMBER Molecular Dynamics Software to Intel's Many Integrated Core (MIC) Architecture. *Comput. Phys. Commun.* **2015**, *201*, 95−105.
(25) Salvalaglio, M.; Perego, C.; Giberti, F.; Mazzotti, M.; Parrinello, M. Molecular-Dynamics Simulations of Urea Nucleation from Aqueous Solution. *Proc. Natl. Acad. Sci. U. S. A.* **2015**, *112* (1), E6−14.
(26) Giberti, F.; Salvalaglio, M.; Mazzotti, M.; Parrinello, M. Insight into the Nucleation of Urea Crystals from the Melt. *Chem. Eng. Sci.* **2015**, *121*, 51−59.
(27) Shah, M.; Santiso, E. E.; Trout, B. L. Computer Simulations of Homogeneous Nucleation of Benzene from the Melt. *J. Phys. Chem. B* **2011**, *115* (35), 10400−10412.
(28) Santiso, E. E.; Trout, B. L. A General Method for Molecular Modeling of Nucleation from the Melt. *J. Chem. Phys.* **2015**, *143* (17), 174109.
(29) Gavezzotti, A. Can a Computer Crystallize a Liquid? Molecular Simulation of Continuous Trajectories from Liquid to Crystalline N-Hexane. *CrystEngComm* **2011**, *13* (10), 3573.
(30) Lauricella, M.; Meloni, S.; English, N. J.; Peters, B.; Ciccotti, G. Methane Clathrate Hydrate Nucleation Mechanism by Advanced Molecular Simulations. *J. Phys. Chem. C* **2014**, *40* (118), 22847−22857.
(31) Parks, C.; Koswara, A.; DeVilbiss, F.; Tung, H.-H.; Nere, N. K.; Bordawekar, S.; Nagy, Z. K.; Ramkrishna, D. Solubility Curves and Nucleation Rates from Molecular Dynamics for Polymorph Prediction − Moving beyond Lattice Energy Minimization. *Phys. Chem. Chem. Phys.* **2017**, *19* (No. 1), 5285.
(32) Banerjee, S.; Briesen, H. Molecular Dynamics Simulations of Glycine Crystal-Solution Interface. *J. Chem. Phys.* **2009**, *131* (18), 184705.
(33) Salvalaglio, M.; Vetter, T.; Giberti, F.; Mazzotti, M.; Parrinello, M. Uncovering Molecular Details of Urea Crystal Growth in the Presence of Additives. *J. Am. Chem. Soc.* **2012**, *134* (41), 17221−17223.
(34) Mandal, T.; Marson, R. L.; Larson, R. G. Coarse-Grained Modeling of Crystal Growth and Polymorphism of a Model Pharmaceutical Molecule. *Soft Matter* **2016**, *12*, 8246−8255.
(35) Salvalaglio, M.; Vetter, T.; Mazzotti, M.; Parrinello, M. Controlling and Predicting Crystal Shapes: The Case of Urea. *Angew. Chem., Int. Ed.* **2013**, *52* (50), 13369−13372.
(36) Piana, S.; Reyhani, M.; Gale, J. D. Simulating Micrometre-Scale Crystal Growth from Solution. *Nature* **2005**, *438* (7064), 70−73.
(37) Piana, S.; Gale, J. D. Understanding the Barriers to Crystal Growth: Dynamical Simulation of the Dissolution and Growth of Urea from Aqueous Solution. *J. Am. Chem. Soc.* **2005**, *127* (6), 1975−1982.
(38) Gao, Y.; Olsen, K. W. Molecular Dynamics of Drug Crystal Dissolution: Simulation of Acetaminophen Form I in Water. *Mol. Pharmaceutics* **2013**, *10* (3), 905−917.
(39) Gao, Y.; Olsen, K. W. Unique Mechanism of Facile Polymorphic Conversion of Acetaminophen in Aqueous Medium. *Mol. Pharmaceutics* **2014**, *11* (9), 3056−3067.
(40) Lanaro, G.; Patey, G. N. Molecular Dynamics Simulation of NaCl Dissolution. *J. Phys. Chem. B* **2015**, *119* (11), 4275−4283.
(41) Greiner, M.; Elts, E.; Briesen, H. Insights into Pharmaceutical Nanocrystal Dissolution: A Molecular Dynamics Simulation Study on Aspirin. *Mol. Pharmaceutics* **2014**, *11* (9), 3009−3016.
(42) Elts, E.; Greiner, M.; Briesen, H. Predicting Dissolution Kinetics for Active Pharmaceutical Ingredients on the Basis of Their Molecular Structures. *Cryst. Growth Des.* **2016**, *16* (7), 4154−4164.
(43) Greiner, M.; Elts, E.; Schneider, J.; Reuter, K.; Briesen, H. Dissolution Study of Active Pharmaceutical Ingredients Using Molecular Dynamics Simulations with Classical Force Fields. *J. Cryst. Growth* **2014**, *405*, 122−130.
(44) Siepmann, J.; Siepmann, F. Mathematical Modeling of Drug Dissolution. *Int. J. Pharm.* **2013**, *453* (1), 12−24.
(45) Joswiak, M. N.; Duff, N.; Doherty, M. F.; Peters, E. Size Dependent Surface Free Energy and Tolman Corrected Droplet Nucleation of TIP4P/2005 Water. *J. Phys. Chem. Lett.* **2013**, *4* (24), 4267−4272.
(46) Bahadur, R.; Russell, L. M.; Alavi, S. Surface Tensions in NaCl - Water - Air Systems from MD Simulations. *J. Phys. Chem. B* **2007**, *111* (41), 11989−11996.
(47) Cheong, D. W.; Boon, Y. Di. Comparative Study of Force Fields for Molecular Dynamics Simulations of α-Glycine Crystal Growth from Solution. *Cryst. Growth Des.* **2010**, *10* (12), 5146−5158.
(48) Berendsen, H. J. C.; van der Spoel, D.; van Drunen, R. GROMACS: A Message-Passing Parallel Molecular Dynamics Implementation. *Comput. Phys. Commun.* **1995**, *91* (1−3), 43−56.
(49) Allen, F. H. The Cambridge Structural Database: A Quarter of a Million Crystal Structures and Rising. *Acta Crystallogr., Sect. B: Struct. Sci.* **2002**, *58* (3 PART 1), 380−388.
(50) Duff, N.; Peters, B. Polymorph Specific RMSD Local Order Parameters for Molecular Crystals and Nuclei: α-, β-, and γ-Glycine. *J. Chem. Phys.* **2011**, *135* (13), 134101.
(51) Plimpton, S. Fast Parallel Algorithms for Short Range Molecular Dynamics. *J. Comput. Phys.* **1995**, *117*, 1−19.
(52) Chisholm, J. A.; Motherwell, S.; Tulip, P. R.; Parsons, S.; Clark, S. J. An Ab Initio Study of Observed and Hypothetical Polymorphs of Glycine. *Cryst. Growth Des.* **2005**, *5* (4), 1437−1442.
(53) Freeman, C. M.; Andzelm, J. W.; Ewig, C. S.; Hill, J.; Delley, B. The Structure and Energetics of Glycine Polymorphs Based on First Principles Simulation Using Density Functional Theory. *Chem. Commun.* **1998**, *2*, 2455−2456.
(54) Marom, N.; Distasio, R. A.; Atalla, V.; Levchenko, S.; Reilly, A. M.; Chelikowsky, J. R.; Leiserowitz, L.; Tkatchenko, A. Many-Body Dispersion Interactions in Molecular Crystal Polymorphism. *Angew. Chem., Int. Ed.* **2013**, *52* (26), 6629−6632.
(55) Yang, X.; Wang, X.; Ching, C. B. Solubility of Form α and Form γ of Glycine in Aqueous Solutions. *J. Chem. Eng. Data* **2008**, *53* (5), 1133−1137.
(56) Bouchard, A.; Hofland, G. W.; Witkamp, G.-J. Solubility of Glycine Polymorphs and Recrystallization of β-Glycine. *J. Chem. Eng. Data* **2007**, *52* (5), 1626−1629.
(57) Towler, C. S.; Davey, R. J.; Lancaster, R. W.; Price, C. J. Impact of Molecular Speciation on Crystal Nucleation in Polymorphic Systems: The Conundrum of γ Glycine and Molecular "Self Poisoning. *J. Am. Chem. Soc.* **2004**, *126* (41), 13347−13353.
(58) Savjani, K. T.; Gajjar, A. K.; Savjani, J. K. Drug Solubility: Importance and Enhancement Techniques. *ISRN Pharm.* **2012**, *2012*, 1−10.


DOI: 10.1021/acs.molpharmaceut.6b00882
*Mol. Pharmaceutics* 2017, 14, 1023−1032